

We are IntechOpen, the world's leading publisher of Open Access books Built by scientists, for scientists

6,900

Open access books available

186,000

International authors and editors

200M

Downloads

Our authors are among the

154

Countries delivered to

TOP 1%

most cited scientists

12.2%

Contributors from top 500 universities



WEB OF SCIENCE™

Selection of our books indexed in the Book Citation Index
in Web of Science™ Core Collection (BKCI)

Interested in publishing with us?
Contact book.department@intechopen.com

Numbers displayed above are based on latest data collected.
For more information visit www.intechopen.com



Mobile Platform with Leg-Wheel Mechanism for Practical Use

Shuro Nakajima

*The Department of Advanced Robotics, Chiba Institute of Technology
Japan*

1. Introduction

Robots that can move over rough terrain with active body leveling are now in strong demand. Such a robot can have a variety of uses, such as carrying packages, assisting people who have difficulty in walking, and safety monitoring outdoors.

Many robots capable of moving over rough terrain exist as research tools; however, few are suitable for practical use. These robots can be generally classified into the three categories.

1) Legged robots: These have excellent mobility with high stability. The mobility of legged robots has been extensively studied: for example, ASV (Song and Waldron 1989), the TITAN series (Hirose et al. 1985), DANTE II (Bares and Wettergreen 1997), the hexapod robot (Delcomyn and Nelson 2000), Tekken2 (Kimura et al. 2007), and Hyperion3 (Yoneda 2007).

2) Wheeled robots: These are most commonly selected for traversing continuous surfaces that include rough terrain. Because of their stability, maneuverability, and simple controls, wheels are the most frequently used mechanism for exploration rovers. Examples of wheeled mobile robots are Micro5 (Kubota et al. 2003), Rocky7 (Volpe et al. 1997), Shrimp (Siegwart et al. 2002), CRAB (Thueer et al. 2006), and Zaurus (Sato et al. 2007). These have passive linkage mechanisms. SpaceCat (Lauria et al. 1998) and Nanokhod (Winnendael et al. 1999) have active linkage mechanisms. The high-grip stair climber (Yoneda et al. 2009) is a crawler-type robot.

3) Leg-wheel robots: These attempt to combine the advantages of both legs and wheels in various configurations. Work Partner (Halme et al. 2003), Roller Walker (Endo and Hirose 2000), Zero Carrier (Yuan and Hirose 2004), Hylos (Grand et al. 2004), and PAW (J.A. Smith et al. 2006) are equipped with wheels placed at the ends of their legs; the Chariot series (Nakajima and Nakano 2008a,b, 2009a-c, Fig. 1), RoboTrac (Six and Kecskem'ethy 1999), and a wheel chair robot (Morales et al. 2006) have separate wheels and legs; Whegs (Quinn et al. 2003; Daltorio et al. 2009) and Epi.q-1 (Quaglia et al. 2010) have four wheels composed of rotating legs or wheels; and Wheeleg (Lacagnina et al. 2003) has two front legs and two rear wheels.

Although a legged robot is highly mobile on rough terrain, the mechanism is complex and more energy is required for walking. On the other hand, while wheeled robots are usually the best solution for continuous terrain, most cannot travel over discontinuous terrain. Generally speaking, a hybrid mechanism like Fig. 1 provides the strengths of both wheels and legs, although such mechanisms tend to be complex. Chariot 3 is equipped with four legs of three degrees of freedom and two independent wheels. On the other hand, Whegs is not complex,



Fig. 1. A leg-wheel robot. (a)Chariot 3. (b)Chari-Bee is a demonstration robot of Aichi EXPO, 2005.

but the posture of its body cannot be easily controlled. PAW has both wheel and leg modes with a simple mechanism and can control its posture in wheel mode by adjusting each leg tip position; however, PAW cannot get over a step statically while maintaining a horizontal posture. The evaluation point for the mechanism in this chapter is to maintain the horizontal posture of the body on rough terrain statically, because a person or object should be carried stably on the robot.

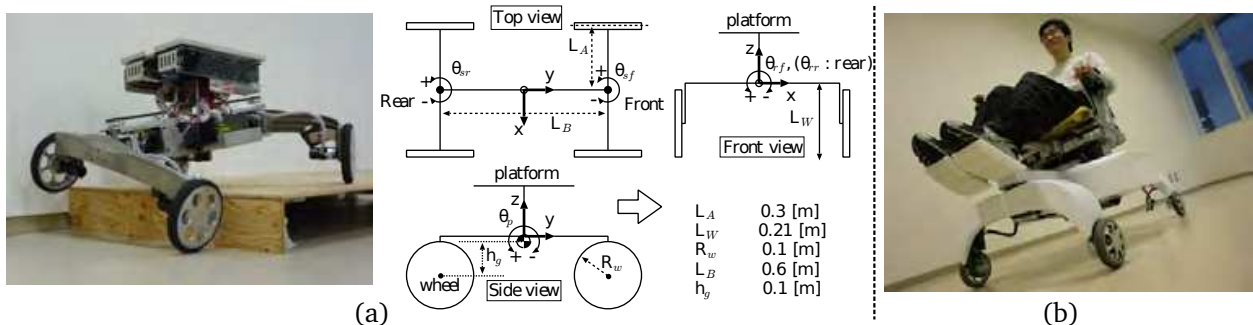


Fig. 2. RT-Mover series. (a)A middle size type. (b)A personal mobility vehicle type.

The proposed robots, the RT-Mover series (Nakajima 2011a, b)(Fig. 2), have a simple mechanism and adequate mobility with a stable posture position for the following target environments: 1. an indoor environment including a step and an uneven ground surface; 2. an artificial outdoor environment with an uneven ground surface and a bump; and 3. natural terrain such as a path in a forest. RT-Mover's mechanism is different from that of conventional mobile robots: four wheels are mounted at the tip of every leg but it has only four active wheels and only five other active shafts. With an emphasis on minimizing the number of drive shafts, the mechanism is designed for a four-wheeled mobile body that is widely used in practical locomotive machinery. RT-Mover can move like a wheeled robot and also walk over a step like a legged robot, despite the simplicity of the mechanism.

The robot can move on discontinuous, rough terrain while maintaining its platform in a horizontal position. Therefore, it can be used as a stable carrier for an object (Fig. 2(a)) or a person (Fig. 2(b)).

In this chapter, the mechanical design concept for RT-Mover is discussed, and strategies for moving on rough terrain are proposed. The kinematics, stability, and control of the robot are also described in detail. The performance of the proposed locomotion is evaluated through simulations and experiments.

2. RT-mover

2.1 Mechanical concept

The target of this chapter is a practical mobile robot that carries objects or people or is used as a mobile bogie for a service robot. It is necessary to keep objects, the upper half of the onboard parts, and the boarding seat (hereinafter, the platform) horizontal in order to carry people and objects. We also aim to develop a practical robot with high cost performance by reducing the number of drive shafts to the extent possible and employing a simple mechanism.

Table 1 shows the practical use status of robots with various locomotion mechanisms. Wheeled robots have been used for practical applications. On the other hand, robots with complex mechanisms are not currently suitable for practical use because they are difficult to control, operate, and maintain, and they are expensive because of their many actuators.

Type	Status
Leg	No examples of practical use to date
Wheel	Some examples of practical use (e.g., cleaning robots)
Crawler	Few examples of practical use (e.g., in leisure and construction fields)
Hybrid mechanism	No examples of practical use to date

Table 1. Practical use status of mobile robots with various locomotion mechanisms

A mobile robot used for general purposes should have high speed on a paved road and good ability of locomotion over rough terrain. Although there is no mechanism superior to a wheel for high speed and energy efficiency, a wheeled robot can move only on continuous rough terrain. To move on discontinuous terrain, a leg mechanism is better than a wheel mechanism. Therefore, to perform all the essential functions of mobile robots in rough terrain, both wheel and leg mechanisms are needed.

Table 2 shows the strengths and limitations of leg-wheel robots. Moreover, the target application environment such as an urban environment is basically a paved surface upon which transportation by wheel is possible, with several steps that necessitate a leg function in order to reach the destination.

Strengths	Ability of locomotion on rough terrain is good because of the use of a leg mechanism.
	High speed movement is possible because of the use of a wheel mechanism.
	Ability of locomotion can be enhanced by using leg and wheel mechanisms cooperatively.
Limitations	There is a danger of collision between the legs of the robot and a person near the robot if the leg's motion space is wide.
	The number of actuators (required for legs) increases, so the cost also rises.
	Reliability and maintainability worsen because of the complexity of the leg mechanism.

Table 2. Strengths and limitations of leg-wheel robots

Therefore, it is advantageous to reduce the complexity of the leg mechanism to a minimum and to limit each leg's motion space.

We take a four-wheeled mobile body often used in practice as the starting point in considering the mechanism of the proposed robot, and from there we develop the proposed mechanism. When seeking a high degree of ability of locomotion on rough terrain in a highly used wheel mode, it is clear that each of the four wheels should generate good driving force. In addition, when driving on rough terrain, each of the wheels of a four-wheeled mobile body is required to be driven independently, since each wheel travels a different route. Accordingly, this discussion is based on a four-wheeled mobile body that drives each wheel independently.

2.2 Mechanical design

Cost, reliability, and maintainability are important for practical mobile bodies. These factors can be evaluated from the number of drive shafts to a certain extent. In other words, using fewer drive shafts tends to lower the cost and simplify the mechanism, which in turn leads to increased reliability and maintainability. The above is evident if a comparison is made between practical transport machinery, such as automobiles and trains, and the mobile robot currently being developed.

Since the objective for the robot developed in this chapter is to add the minimum leg functions necessary, a mechanism that minimizes the number of added drive shafts is designed. Specifically, after listing possible mechanisms for each function, the mechanism with the minimum number of drive shafts is chosen for the proposed robot with consideration of the possible combinations.

2.2.1 Steering function

Practical mechanisms to achieve a steering function for a four-wheeled mobile body are shown in Fig. 3(a). Needless to say, there are other mechanisms to achieve steering, but we aim to realize a practical mobile robot. Accordingly, the following discussion targets highly practical representative mechanisms. The mechanism of 1-1 is the Ackermann steering system, an automobile steering system. That of 1-3 is a mechanism that rotates the center of a shaft to steer. It is possible to attach a steering mechanism to the rear wheels of both 1-1 and 1-3. However, this case is the same as 1-1 and 1-3 and is omitted from following discussion. Those of 1-2 and 1-4 are 4-Wheel Steering (4WS) systems in which the four wheels can be directed.

2.2.2 Suspension function in wheel mode

The wheels are required to have active vertical travel according to terrain in order to keep the platform horizontal when moving on gently varying irregular terrain. Systems to fulfill this requirement are shown in Fig. 3(b). The mechanism of 2-1 provides an up-down function to each wheel. The necessary number of drive shafts is four, and the platform can be kept horizontal on rough terrain by the vertical movement of each wheel according to the ground surface.

The mechanism of 2-2 is a bogie mechanism for the left and right wheel that uses a rotating shaft as a drive shaft. The horizontal degree of the roll direction of the platform can be maintained by the active control of the rotating shaft of front and rear bogie mechanism in response to the ground surface. The horizontal degree of the pitch direction of the platform is maintained by attaching an independent pitch control shaft. The number of necessary drive shafts is three.

The mechanism of 2-3 is a bogie mechanism for the front and back wheels.

2.2.3 Suspension mechanism in leg mode

The following factors are necessary for traveling in leg mode over steps and other such obstacles, which cannot be traversed in wheel mode, while maintaining the platform in a horizontal plane: 1. lifting, moving forward, and landing for each leg; 2. supporting the body with three other legs.

The up-and-down function of each leg is achieved by a wheel mode suspension function. The mechanisms to move each wheel back and forth are shown in Fig. 3(c). The mechanism of 3-1 is a method to affix a back-and-forth drive function to each wheel, and the number of required drive shafts is four. That of 3-2 is the same as steering mechanism 1-4, with the wheels moving back-and-forth through rotation of the center shaft. Both 3-1 and 3-2 can locate the center of gravity of the body in the support polygon and thus support the body by shifting to the front and rear of the landing points of the three legs.

2.2.4 Mechanism of proposed robot

The realistically possible combinations of each aforementioned mechanism are examined, and the combinations with the minimum number of drive shafts are determined.

The combinations of each mechanism are listed in Table 3. Impossible or unavailable combinations are indicated by “-”.

As mechanism 3-2 is the same as that of 1-4, it is also a steering mechanism. Therefore, 3-2 cannot be combined with 1-1, 1-2, and 1-3 because this would result in unnecessarily duplicating steering functions in equipping the drive shaft. The mechanism by which to move the wheels back and forth is duplicated in the combination of 1-4 and 3-1, so they are not combined. Also, the simultaneous employment of 1-3 and 2-3, or 1-4 and 2-3, results in a physical contradiction because the distance between front and rear wheels is altered, and these are fixed by the bogie mechanism.

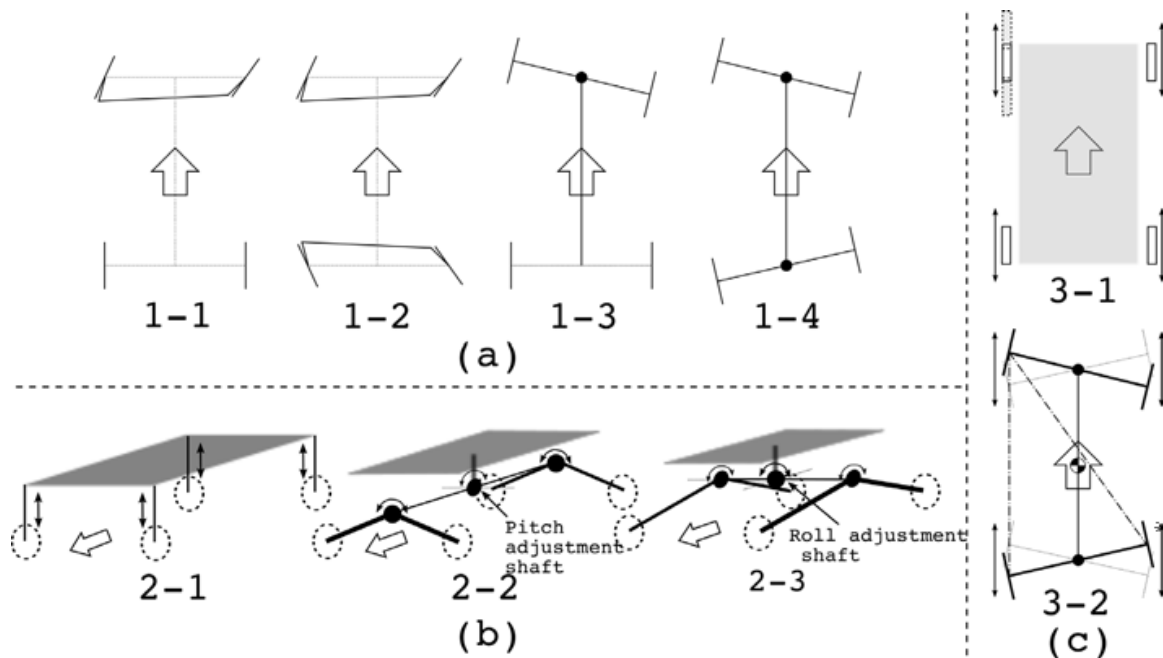


Fig. 3. Mechanism for each function. (a)Steering mechanism. (b)Suspension mechanism for wheel mode. (c)Suspension mechanism for leg mode (Top view).

Steering	Suspension (wheel mode)	Suspension (leg mode)	Number of drive shafts
1-1	2-1	3-1 / 3-2	9 / -
	2-2	3-1 / 3-2	8 / -
	2-3	3-1 / 3-2	8 / -
1-2	2-1	3-1 / 3-2	10 / -
	2-2	3-1 / 3-2	9 / -
	2-3	3-1 / 3-2	9 / -
1-3	2-1	3-1 / 3-2	7 / -
	2-2	3-1 / 3-2	6 / -
	2-3	3-1 / 3-2	- / -
1-4	2-1	3-1 / 3-2	- / 6
	2-2	3-1 / 3-2	- / 5
	2-3	3-1 / 3-2	- / -

Table 3. Combinations of each mechanism

The reason the combination of 1-3, 2-1, and 3-1 results in seven drive shafts is because the front wheels are able to move back and forth by the steering function of 1-3, and only the rear wheels are required to be moved by mechanism 3-1.

As shown in Table 3, the combination of 1-4, 2-2, and 3-2 gives five drive shafts, which is a minimum. Taken together, the mechanism of the proposed robot consists of four drive wheels and five drive shafts, as shown in Fig. 4. The mechanism that has an intersection of the roll-adjustment axis and the steering axis at the center of the steering arm is called the leg-like axle.

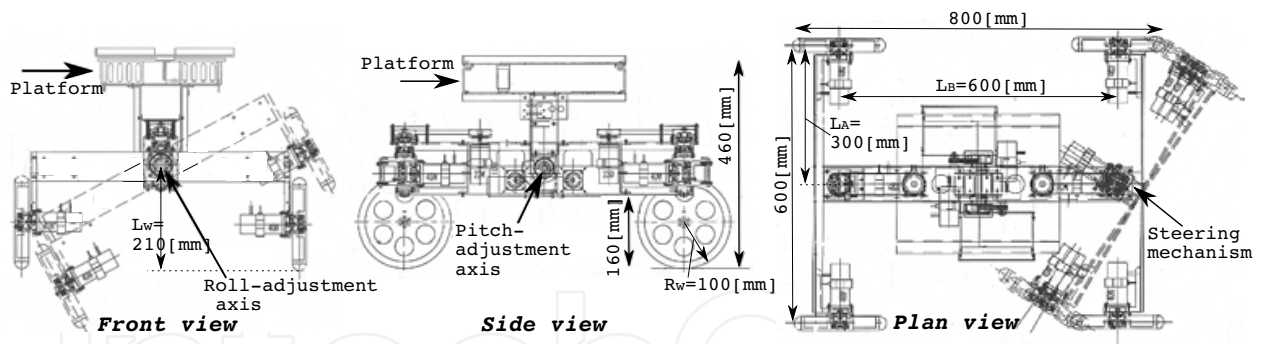


Fig. 4. Assembly drawing of RT-Mover

2.2.5 Consideration of major dimensions

The size of the robot (Fig. 2(a)) is suitable for transporting small objects or serving as a mobile bogie of a service robot. The target is to traverse steps about 0.07 [m] high in wheel mode and 0.15 [m] high in leg mode, on the assumption that a robot of this size would be used in indoor offices, factories, and public facilities. Although depending on the coefficient friction with the floor surface, the wheel mechanism allows the robot to traverse a floor surface with irregularities having height up to about $2/3$ of the wheel radius. Accordingly, the wheel radius for the robot being developed is configured to 0.1 [m].

The specifications of the robot are listed in Table 4.

Dimensions	Length 0.8[m]; Width 0.63[m] (Tread 0.6[m]); Height 0.46[m]; Height to bottom 0.16[m]
Wheel	Radius:0.1[m]; Width:0.03[m]
Weight	28[kg] (including the platform at 6.5[kg] and batteries at 5.4[kg])
Motor (DC servo)	23[W] (front and rear steering $\theta_{sf}, \theta_{sr}: \times 2$) 40[W] (front and rear roll $\theta_{rf}, \theta_{rr}: \times 2$; pitch $\theta_p: \times 2$ (double motor); each wheel: $\times 4$)
Gear ratio	100 (steering θ_{sf}, θ_{sr} , and roll θ_{rf}, θ_{rr})
	250 (pitch θ_p)
	50 (each wheel)
Sensor	Encoder (each motor)
	Current sensor (each motor)
	Posture angle sensor (roll and pitch of platform)
Angle limit	± 30 (steering θ_{sf}, θ_{sr} , roll θ_{rf}, θ_{rr} , and pitch θ_p)
Minimum rotation radius	0.52[m]
Max speed	0.63[m/s]
Power supply	24[V] lead accumulator

Table 4. Main specifications

The length of the steering arm (tread) was 0.6 [m], and the maximum angle for steering, roll-adjustment axis, and pitch-adjustment axis was ± 30 [deg]. When rotating the roll-adjustment axis through 30[deg] such that the wheel on one side is in contact with the ground, the other wheel attached to a 0.6[m] steering arm can rise 0.3[m]. Therefore, the movement range is sufficient for this initial step. Likewise, moving 0.3[m] in the front and rear directions is possible by moving the steering from 0[deg] to 30[deg], and holes of 0.3[m] can be crossed (Fig. 7(c)). Also, the radius of rotation is 0.52[m] if the front and rear steering angles are turned a full 30[deg] in antiphase. With regards to locomotion on a slope, back-and-forth movement and traversal of a slope of up to 30[deg] is possible.

3. Control method in wheel mode

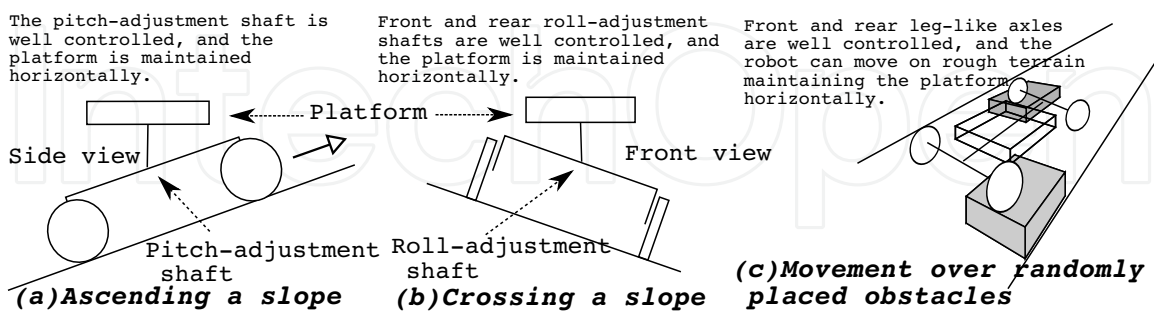


Fig. 5. Wheel mode locomotion

The movement method in wheel mode is shown in Fig. 5. RT-Mover can move on continuous rough terrain while maintaining the platform in a horizontal plane by applying eq. (1) to the pitch-adjustment shaft θ_p , and to the front and rear roll-adjustment shafts θ_{rf}, θ_{rr} .

$$T_d = K(\theta_d - \theta) + D(\dot{\theta}_d - \dot{\theta}) = -K\theta - D\dot{\theta}, \tag{1}$$

where T_d is the target torque, θ is the posture angle of the platform, θ_d : target posture angle of the platform ($= 0$), K is the angle gain, and D is the angular velocity gain.

3.1 Assessment of ability of locomotion in wheel mode

The situations of (a) and (b) shown in Fig. 5 partially appear in (c). Therefore, Fig. 5(c) alone is evaluated by simulation. The conditions employed in the simulation are as follows. Each gain value is obtained experimentally. For the initial step of the study, the velocity is set such that movement in the static state is possible. Since high speeds are a characteristic of wheel driving systems, traveling states with dynamic behavior will be studied in the near future.

1. $K_p = 800[\text{N}\cdot\text{m}]$, $D_p = 15[\text{N}\cdot\text{m}\cdot\text{s}]$, $K_{rf} = K_{rr} = 250[\text{N}\cdot\text{m}]$, $D_{rf} = D_{rr} = 10[\text{N}\cdot\text{m}\cdot\text{s}]$.
2. The speeds of all the wheels are maintained at a constant $0.2[\text{m/s}]$.
3. The front and rear steering angles are maintained at 0 .
4. The wheels and steering are controlled using a proportional derivative (PD) controller.
5. The coefficient of friction between wheel and road is 0.7 , and there is no friction on the shafts of the robot.
6. Open Dynamics Engine (ODE) is used for simulation.

Figure 6 shows a simulation of moving from point A to B in Fig. 6(a) over randomly placed obstacles. In (b) and (c) we see that each adjustment shaft is controlled appropriately, as well as that the platform's posture angle remains horizontal to within $\pm 0.8[\text{deg}]$. This shows that in wheel mode the platform can move over rough terrain with obstacles about $2/3$ the size of the wheel radius as shown in the figure.

When a wheel hits an obstacle, the steering shaft is turned because of the reaction force from the obstacle. If the robot is required to move exactly straight, it is necessary to adjust the corresponding wheel speed according to both the rotation angle of the steering shaft and that of the roll-adjustment shaft. This is a subject for future study.

4. Gait strategy and control method in leg mode

The leg mode locomotion method is shown in Fig. 7. As an initial step, evaluations are performed by simulations and experiments taking Fig. 7 (a) and (b) as examples.

In the future, a method for integrating external sensor information with the robot system will be studied because, for example, such information is necessary to recognize a downward step before descending in Fig. 7(b). At the current stage, road shapes are known in advance.

4.1 Step-up gait

Using the control method in eq. (1), RT-Mover can move over rough terrain where its wheels can be in continuous contact with the ground. However, with steps higher than the wheel radius or gaps larger than the wheel diameter, the ground contact points of wheels need to be altered by lifting the wheels. The case of lifting a wheel onto a step which the robot cannot climb in wheel mode is shown in Fig. 8. Assuming that static stability is maintained, a wheel is lifted like a leg while the body is constantly supported on at least three wheels.

Figure 9 shows the flow of the step-up gait. Before and after an upward step, the robot runs in wheel mode (Fig. 9(a) and (l)). When a front wheel reaches the step, the rear steering is rotated so that the margin of static stability during leg motion increases (Fig. 9(b)). Since RT-Mover cannot adjust the position of its center of gravity due to having a small number of degrees of

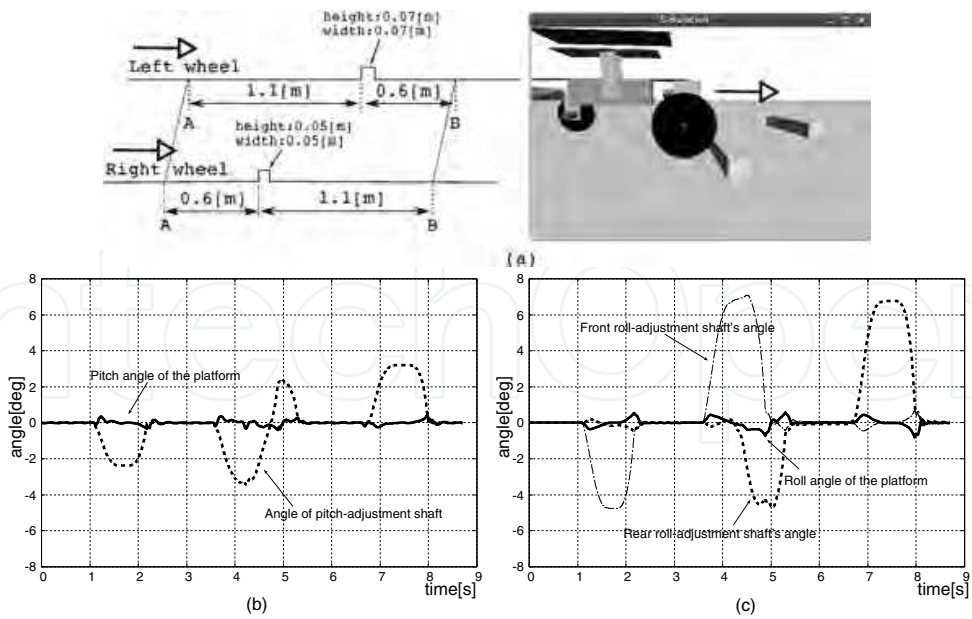


Fig. 6. Simulation of moving over randomly placed obstacles. (a) Shape of the road and a scene from the simulation. (b) Platform's pitch and the angle of the pitch-adjustment shaft. (c) Data on platform's roll and the angles of the front and rear roll-adjustment shafts for the movement from point A to B in (a).

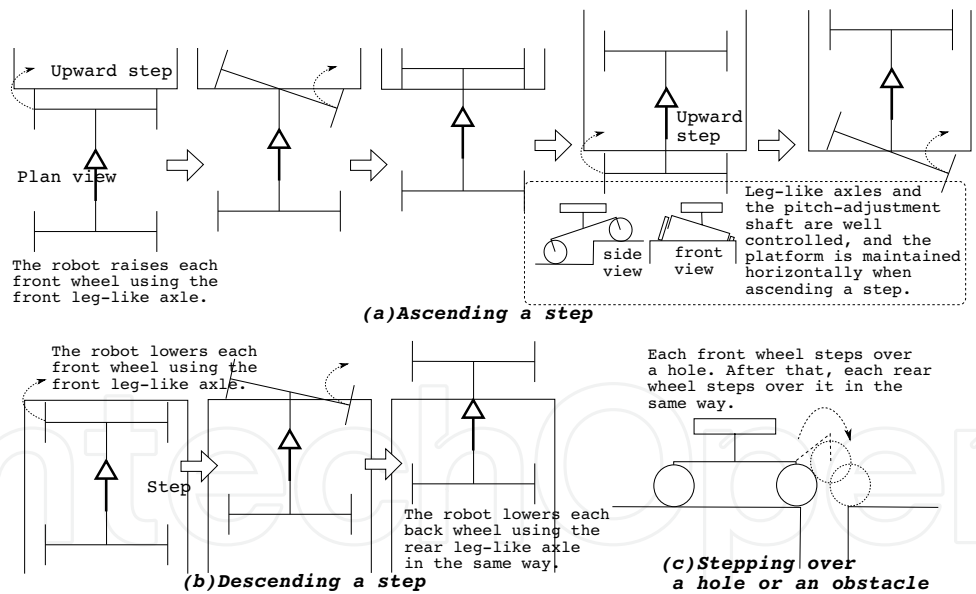


Fig. 7. Leg mode locomotion

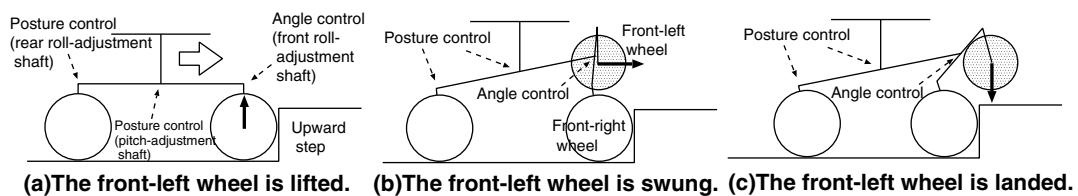


Fig. 8. Leg motion of front-left wheel

freedom, the positions of supporting wheels are adjusted by rotating a steering shaft in order to maintain static stability. Since the leg-side steering shaft is used for moving the lifted wheel forward, static stability is increased by rotating the support-side steering shaft to the limit ($-30[\text{deg}]$). In order to lift a leg, the front roll-adjustment shaft is switched from posture control (eq. (1)) to angle control, and the leg is lifted to the desired height (Fig. 8(a)). Meanwhile, to prevent the platform from inclining, the rear roll-adjustment shaft and pitch-adjustment shaft continue to use posture control. After lifting, the angle of the front roll-adjustment shaft is kept constant, and the lifted wheel is moved forward onto the step (Fig. 8(b) and Fig. 9(c)). Then, the lifted wheel is lowered, and when landing is detected, leg motion of the front-left wheel ends (Fig. 8(c)). As can be seen in Fig. 18(a), since the sign of the roll angle of the platform changes from negative to positive at (A) when the wheel lands, this timing can be used for detection. Next, the front-right wheel becomes the lifted leg (Fig. 9(d) and (e)). After the front wheels have gone up the step, the robot changes its yaw angle relative to the step to ensure static stability when the rear wheels go up (this is considered in detail in a later section). The robot moves forward keeping the rear steering angle at $30[\text{deg}]$ until its yaw angle reaches the desired value (Fig. 9(f)). After that, it moves forward in wheel mode while maintaining the desired yaw angle (Fig. 9(g) and (h)). When a rear wheel reaches the step, the rear wheels are lifted onto the step in the same way as the front wheels (Fig. 9(i) and (j)). The rear roll-adjustment shaft is controlled using angle control, and the front one by posture control. Finally, the robot changes its yaw angle back to 0 (Fig. 9(k)). Since the left-right order does not affect this movement, each wheel is lifted in turn in the order front-left, front-right, rear-left, and rear-right.

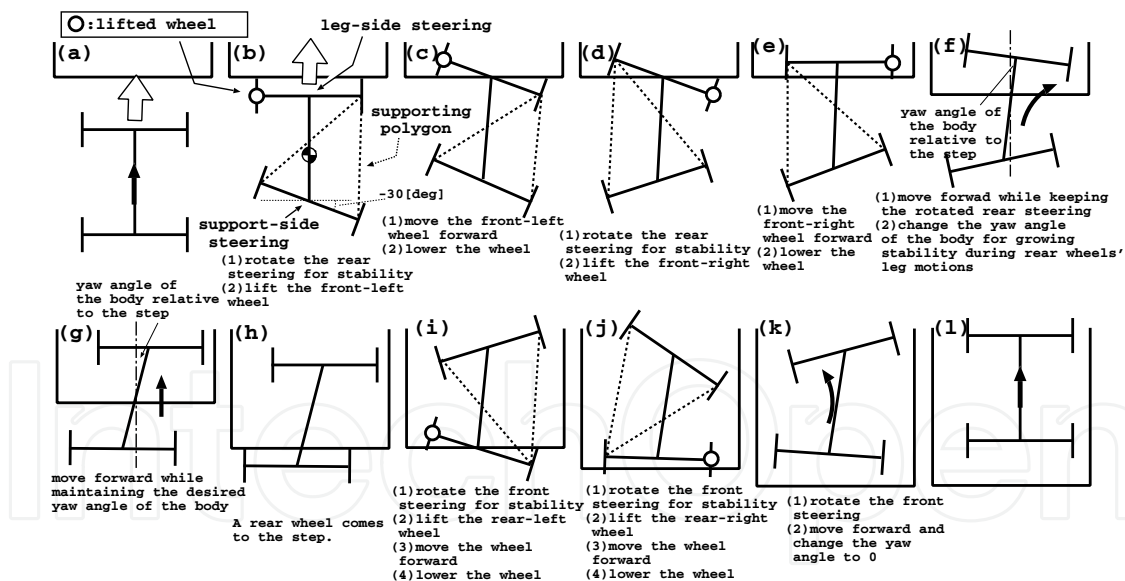


Fig. 9. Flow of processes in the step-up gait

4.2 Step-down gait

Figure 10 shows the flow of the step-down gait. When all wheels support the body, the robot is controlled under wheel mode.

When a front wheel encounters a downward step, the robot changes the yaw angle of its body relative to the step for ensuring static stability. So, after the robot reaches the step for the first time (Fig. 10(a)), it moves backward keeping the rear steering angle at $-30[\text{deg}]$ until

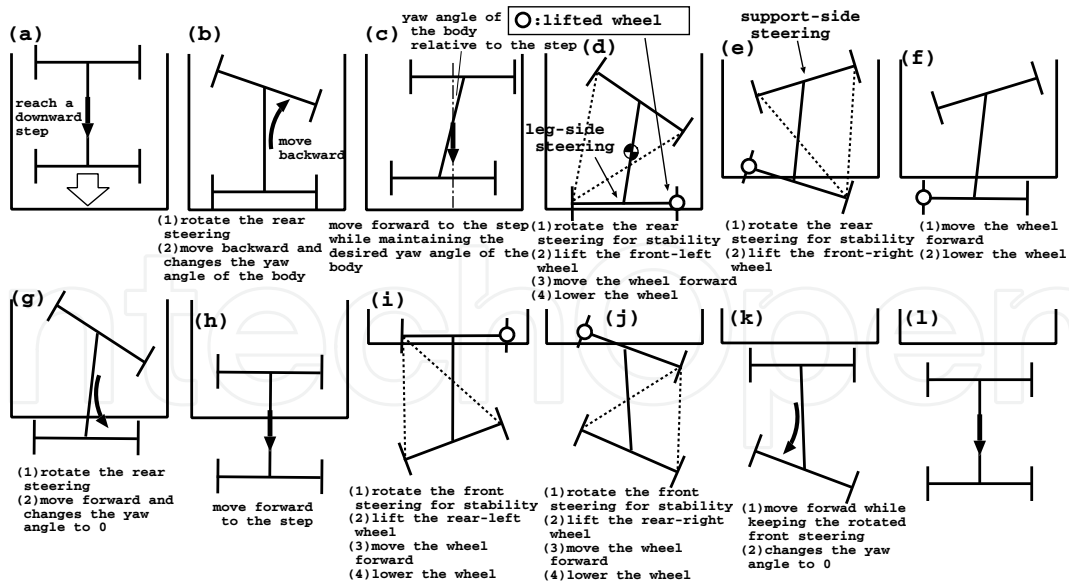


Fig. 10. Flow of processes in the step-down gait

the yaw angle of its body relative to the step acquires the desired value (Fig. 10(b)). Then, it moves forward to the step maintaining this yaw angle (Fig. 10(c)). When a front wheel reaches the step, the rear steering is rotated so that the margin of static stability during leg motion increases (Fig. 10(d)). First, the front-left leg is lifted (Fig. 10(d)), then the front right-leg is lifted (Fig. 10(e) and (f)). After both front wheels have completed the leg motion, the robot changes its yaw angle back to 0[deg] relative to the step (Fig. 10(g)). The yaw angle at this time is not important, because the static stability is sufficient during the rear wheels' leg motion. After coming to the step (Fig. 10(h)), the rear wheels are lifted down in the same way as the front wheels (Fig. 10(i) and (j)). Finally, the robot again changes the yaw angle of its body to 0 (Fig. 10(k)). The roll-adjustment shaft on the leg side is controlled using angle control, and that on the support side uses posture control.

5. Inverse kinematics

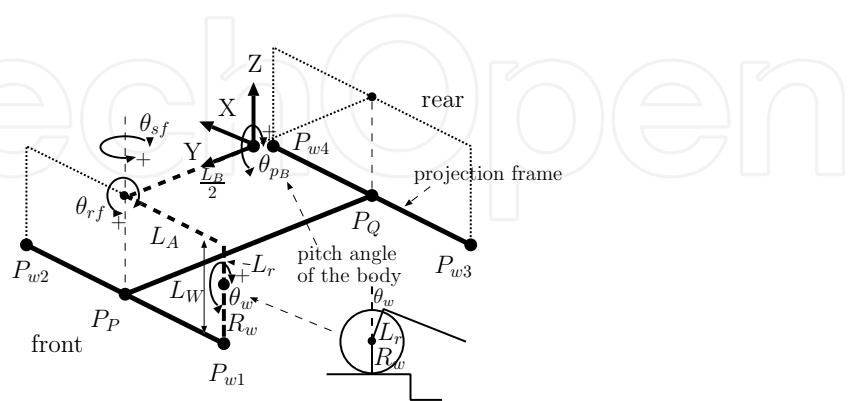


Fig. 11. Frame model for analysis

In this section, the target angle of each joint shaft to achieve the configured leg tip trajectory and the target angle of each wheel when in wheel mode are obtained. In other words, in leg

mode, for example, the inverse kinematics to achieve the trajectory by lifting the transfer leg vertically, swinging it forward, and setting it down vertically to land is described.

A “projection frame” is introduced (Fig. 11), which comprises projecting line segments connecting the wheel supporting points (front arm $P_{w1}P_{w2}$, and rear arm $P_{w3}P_{w4}$) and a line segment connecting the centers of the arms (body $P_P P_Q$) to a horizontal plane. Here, the inverse kinematics are discussed using this projection frame. We use a right-handed coordinate system with the center of the projection frame as the origin. The direction of travel is defined as Y and the vertical axis as Z. Then, the following matrix ${}^0T_{w_{f1}}$ maps to coordinates with the front-left leg at the origin of the body-centered coordinate system:

$${}^0T_{w_{f1}} = \begin{pmatrix} 1 & 0 & 0 & 0 \\ 0 & C\theta_{p_B} & -S\theta_{p_B} & 0 \\ 0 & S\theta_{p_B} & C\theta_{p_B} & 0 \\ 0 & 0 & 0 & 1 \end{pmatrix} \begin{pmatrix} 1 & 0 & 0 & 0 \\ 0 & 1 & 0 & \frac{L_B}{2} \\ 0 & 0 & 1 & 0 \\ 0 & 0 & 0 & 1 \end{pmatrix} \begin{pmatrix} C\theta_{sf} & -S\theta_{sf} & 0 & 0 \\ S\theta_{sf} & C\theta_{sf} & 0 & 0 \\ 0 & 0 & 1 & 0 \\ 0 & 0 & 0 & 1 \end{pmatrix} \begin{pmatrix} C\theta_{rf} & 0 & S\theta_{rf} & 0 \\ 0 & 1 & 0 & 0 \\ -S\theta_{rf} & 0 & C\theta_{rf} & 0 \\ 0 & 0 & 0 & 1 \end{pmatrix} \begin{pmatrix} 1 & 0 & 0 & -L_A \\ 0 & 1 & 0 & 0 \\ 0 & 0 & 1 & 0 \\ 0 & 0 & 0 & 1 \end{pmatrix} \begin{pmatrix} 1 & 0 & 0 & 0 \\ 0 & 1 & 0 & 0 \\ 0 & 0 & 1 & -L_r \\ 0 & 0 & 0 & 1 \end{pmatrix} \begin{pmatrix} 1 & 0 & 0 & 0 \\ 0 & C\theta_w & -S\theta_w & 0 \\ 0 & S\theta_w & C\theta_w & 0 \\ 0 & 0 & 0 & 1 \end{pmatrix} \begin{pmatrix} 1 & 0 & 0 & 0 \\ 0 & 1 & 0 & 0 \\ 0 & 0 & 1 & -R_w \\ 0 & 0 & 0 & 1 \end{pmatrix}. \quad (2)$$

5.1 Lifting and landing phases

When lifting or landing the front-right wheel, an angular velocity value will be determined for the front roll-adjustment shaft. In order to avoid contacting a lateral surface of the step, the lifted wheel is moved up and down without moving back or forth. The posture control given by eq. (1) is applied to the pitch adjustment and rear roll-adjustment shafts, and the rotation of the supporting front-left wheel is stopped. In order to widen the supporting polygon, the rear steering shaft is rotated to its steering limit. The control parameters of the front steering shaft, the rear-left wheel, and the rear-right wheel are determined by the value set for the front roll-adjustment shaft.

The derivation of these three control parameters is described in an absolute coordinate system with its origin at the supporting position of the front-left wheel $P_{w1}(t)$, as shown in Fig. 12(a). In Fig. 12(a), the position of the front-right wheel $P_{w2}(t)$ and $P_{w2}(t + \Delta t)$, when rotating the front roll-adjustment shaft for a small amount of time Δt , are calculated. The angular velocity of the front steering shaft, $\dot{\theta}_{sf}(t)$, and the velocities of the rear-left and rear-right wheels, $\mathbf{V}_{w3}(t)$ and $\mathbf{V}_{w4}(t)$, are also derived. Since the wheel is moved up and down without moving in the Y direction, the Y coordinate of P_P is constant.

The distance between $P_{w1}(t)$ and $P_P(t)$ is $A_f(t)$; since this is half the distance between $P_{w1}(t)$ and $P_{w2}(t)$, it may be derived from eq. (2). According to eq. (2), $A_f(t)$ depends on the front steering $\theta_{sf}(t)$, the front roll axis $\theta_{rf}(t)$, and the body pitch angle $\theta_{p_B}(t)$. The value of A_f after a small incremental movement of $\theta_{rf}(t)$ is $A_f(t + \Delta t)$. Because an analytic solution is difficult, θ_{sf} and θ_{p_B} are approximated as not varying over time Δt . Since the Y axis moves in a fixed up and down path, the Y coordinate of P_{w2} is fixed and is given below:

$$(P_{w2x}(t), P_{w2y}(t)) = (2A_f(t) \cos(\theta_{leg}(t) + \theta_B(t)), 2A_f(t) \sin(\theta_{leg}(t) + \theta_B(t))), \quad (3)$$

$$(P_{w2x}(t + \Delta t), P_{w2y}(t + \Delta t)) = (\sqrt{4A_f(t + \Delta t)^2 - P_{w2y}(t)^2}, P_{w2y}(t)), \quad (4)$$

$\theta_{leg}(t)$ and $\theta_B(t)$ are obtained by eqs. (6), (7), and (10), when their initial values are given.

The velocity of P_P and the small angle $\Delta\theta_o(t)$ are given by

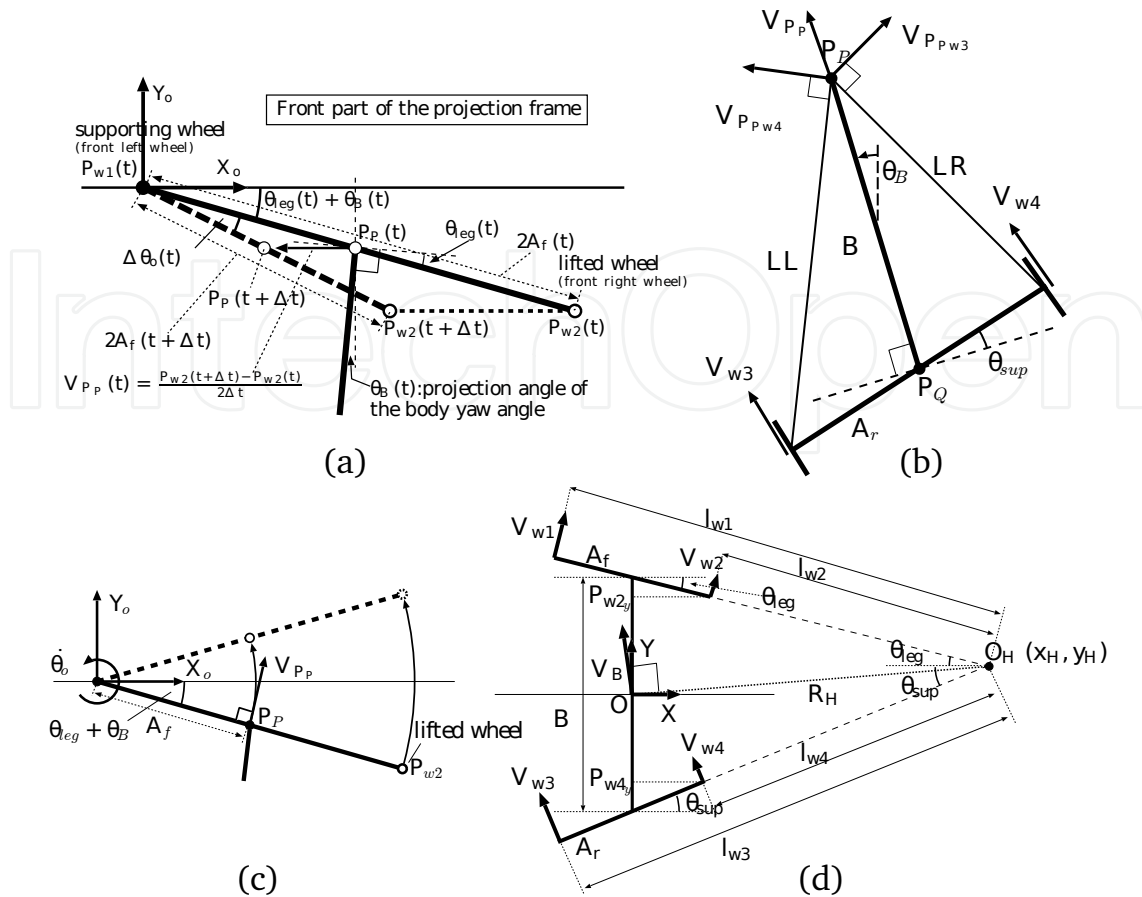


Fig. 12. Calculation model. (a) For the trajectory of a leg tip when raising and lowering a wheel. (b) For V_{w3} and V_{w4} . (c) For swing phase. (d) For wheel mode.

$$\mathbf{V}_{P_P}(t) = (V_{P_{px}}(t), V_{P_{py}}(t)) = \left(\frac{P_{w2x}(t + \Delta t) - P_{w2x}(t)}{2\Delta t}, 0 \right), \tag{5}$$

$$\Delta\theta_o(t) = -\tan^{-1} \frac{P_{w2y}(t)}{P_{w2x}(t)} - \tan^{-1} \frac{P_{w2y}(t + \Delta t)}{P_{w2x}(t + \Delta t)}. \tag{6}$$

$\Delta\theta_o(t)$ is the sum of the changes in the projected front steering angle $\theta_{leg}(t)$ and the body yaw angle $\theta_B(t)$:

$$\Delta\theta_o(t) = \Delta\theta_{leg}(t) + \Delta\theta_B(t). \tag{7}$$

From these variables, the angular velocity of the projected front steering shaft $\dot{\theta}_{leg}(t)$ and the angular velocity of the front steering $\dot{\theta}_{sf}(t)$ are determined by calculating $\dot{\theta}_B(t)$ and using the relationship between $\dot{\theta}_{leg}(t)$ and $\dot{\theta}_{sf}(t)$, which is determined topologically from the relations below.

$$\theta_{leg}(t) = \theta_{sf}(t) \cos \theta_{p_B}(t) + \theta_{rf}(t) \sin \theta_{p_B}(t), \tag{8}$$

$$\therefore \dot{\theta}_{sf}(t) = \frac{\dot{\theta}_{leg}(t) - \dot{\theta}_{rf}(t) \sin \theta_{p_B}(t) + \dot{\theta}_{p_B}(t) (\theta_{sf}(t) \sin \theta_{p_B}(t) - \theta_{rf}(t) \cos \theta_{p_B}(t))}{\cos \theta_{p_B}(t)}, \tag{9}$$

where θ_{p_B} is obtained from attitude sensor information on the platform and the pitch adjustment angle.

The angular velocity of the body rotation $\dot{\theta}_B$ is

$$\dot{\theta}_B(t) = \frac{V_{P_{Qx}}(t) - V_{P_{Px}}(t)}{B(t)}, \quad (10)$$

where B is the length of the projection body and $V_{P_{Qx}}$ is the x element of the velocity of P_Q (Fig. 12(b)). $B(t)$ is the length between 0P_P and 0P_Q , where 0P_P and 0P_Q are the positions of P_P and P_Q in the body-centered coordinate system. The velocity of P_Q , \mathbf{V}_{P_Q} , is given by

$$\mathbf{V}_{P_Q}(t) = ({}^0\mathbf{P}_Q(t) - {}^0\mathbf{P}_Q(t - \Delta t) - \Delta\mathbf{O}_o) / \Delta t, \quad (11)$$

where $\Delta\mathbf{O}_o$ is the movement of the origin of the body-centered coordinate system relative to the absolute coordinate system:

$$\Delta\mathbf{O}_o = {}^0\mathbf{P}_{w1}(t) - {}^0\mathbf{P}_{w1}(t - \Delta t). \quad (12)$$

The angular velocity of the front steering shaft $\dot{\theta}_{sf}$, which is one of the three control parameters, is determined by eqs. (6), (7), (9), and (10).

5.1.1 How to derive velocities of rear-left and rear-right wheel

Here, we derive the velocities of the rear-left and rear-right wheels, $\mathbf{V}_{w3}(t)$ and $\mathbf{V}_{w4}(t)$. The velocity generated at point P_P when stopping the right-back wheel ($\mathbf{V}_{w4} = 0$) and moving left-back wheel at \mathbf{V}_{w3} is $\mathbf{V}_{P_{Pw3}}$ shown in Fig. 12(b). If we define $\mathbf{V}_{P_{Pw4}}$ similarly, then the velocity of $P_P(t)$ is

$$\mathbf{V}_{P_P}(t) = \mathbf{V}_{P_{Pw3}}(t) + \mathbf{V}_{P_{Pw4}}(t). \quad (13)$$

The relationships between \mathbf{V}_{w3} and $\mathbf{V}_{P_{Pw3}}$, and between \mathbf{V}_{w4} and $\mathbf{V}_{P_{Pw4}}$ are

$$\mathbf{V}_{w3}(t) = \frac{2A_r(t)}{LR(t)} \mathbf{V}_{P_{Pw3}}(t), \quad (14)$$

$$\mathbf{V}_{w4}(t) = \frac{2A_r(t)}{LL(t)} \mathbf{V}_{P_{Pw4}}(t), \quad (15)$$

where $LR(t)$ and $LL(t)$ are obtained from $B(t)$, $\theta_{sup}(t)$, and the distance $A_r(t)$ between $P_{w3}(t)$ and $P_Q(t)$ in Fig. 12(b).

The velocities of the rear-left wheel and the rear-right wheel are determined by eqs. (5), (13), (14), and (15).

5.2 Swing phase

Figure 12(c) shows a model of the swing phase, where the origin of the absolute coordinate system is the front-left wheel and the lifted wheel is the front-right wheel. The trajectory is set such that point P_P draws a circular path around the front-left wheel. The angular velocity of the front steering shaft and the velocities of the rear wheels are determined so that they produce \mathbf{V}_{P_P} . Setting a command value for $\dot{\theta}_o$, we obtain

$$|\mathbf{V}_{P_P}(t)| = A_f(t) |\dot{\theta}_o|, \quad (16)$$

$$\mathbf{V}_{P_P}(t) = (-|\mathbf{V}_{P_P}(t)| \sin(\theta_{leg}(t) + \theta_B(t)), |\mathbf{V}_{P_P}(t)| \cos(\theta_{leg}(t) + \theta_B(t))). \quad (17)$$

With the velocity of point P_P determined, as in the lifting and landing phases, the three control parameters, the angular velocity of the front steering shaft and the velocities of the rear wheels, can be obtained.

5.3 Wheel mode

In Fig. 9(g) and (h), for example, the robot moves with all four wheels supporting the body. Since the velocity of the body center, \mathbf{V}_B , and the angles of the front and rear steering axes in the projection frame, θ_{leg} and θ_{sup} , are given as parameters, the desired wheel velocities with no slipping, $\mathbf{V}_{w1} \sim \mathbf{V}_{w4}$, are derived. Since each wheel rotates about O_H , \mathbf{V}_{wi} is given by $\mathbf{V}_{wi}(t) = l_{wi}(t)\mathbf{V}_B(t)/R_H(t)$ ($i = 1 \sim 4$) where $R_H(t)$ is the turning radius. Except under conditions, such as $\theta_{leg} = \theta_{sup}$, where the front and rear steering angles are equal and the turning radius becomes infinite, the topology in Fig. 12(d) leads to

$$O_H(t) = (x_H(t), y_H(t)) = \left(\frac{B(t)}{\tan \theta_{sup}(t) - \tan \theta_{leg}(t)}, \frac{B(t) \tan \theta_{sup}(t) + \tan \theta_{leg}(t)}{2 \tan \theta_{sup}(t) - \tan \theta_{leg}(t)} \right) \quad (18)$$

and $R_H(t) = \sqrt{x_H(t)^2 + y_H(t)^2}$. Variables such as l_{w1} are obtained in the form $l_{w1}(t) = |(x_H(t) - P_{w1x}(t))/\cos \theta_{leg}(t)|$.

However, when $\theta_{leg}(t) = \theta_{sup}(t)$, we have $\mathbf{V}_{wi} = \mathbf{V}_B$ ($i = 1 \sim 4$).

6. Stability in leg mode

In this section, whether the robot can maintain static stability while moving over a target step of 0.15[m] is analyzed for the gait strategy given above. Static state locomotion is considered as an initial step. In general, statically stable locomotion can be achieved if the center of gravity is located inside the support polygon. Here, the stability during movement of the proposed robot in leg mode is specifically investigated. For example, the best range of body yaw angle shown in Fig. 9(g) to climb a step while maintaining stability is derived.

Figure 13(a) shows the static stability when lifting the front-left wheel. Static stability is positive if the center of gravity is in the supporting polygon. Since RT-Mover employs a mechanism with a small number of driving shafts, it cannot move its center of gravity without altering the position of the supporting wheels. In addition, the supporting point of the front-right wheel in Fig. 13(a) cannot move since the lifted wheel is needed to move forward. Thus, the rear steering is used so that the center of gravity stays within the supporting polygon. As shown in Fig. 13(b), if the body inclines backward when going up a step, the center of gravity is displaced backward by $h_g \sin \theta_{p_B}$, where θ_{p_B} is the body pitch angle.

Figure 14(A) shows four phases during the step-up gait. Out of the four phases in which a wheel is lifted during the step-up gait, only those shown in Fig. 14(A-c) and (A-d) cause static instability, because the center of gravity is displaced backward due to the backward inclination of the body and the stability margin consequently decreases. Here, the front steering is rotated up to the limit of ± 30 [deg] in the direction that increases stability. First, the rear-left wheel is lifted (Fig. 14(A-c)), moved forward, and then lowered. Next, the rear-right wheel is lifted, moved forward, and lowered. Therefore, the rear steering angle when the rear-right wheel is lifted depends on the rear steering angle when the rear-left wheel is lifted. It can be seen in Fig. 14(A-c) and (A-d) that the less the lifted rear-left wheel goes forward, the more static stability the robot has at the beginning of lifting the rear-right wheel. Hence, the rear-left

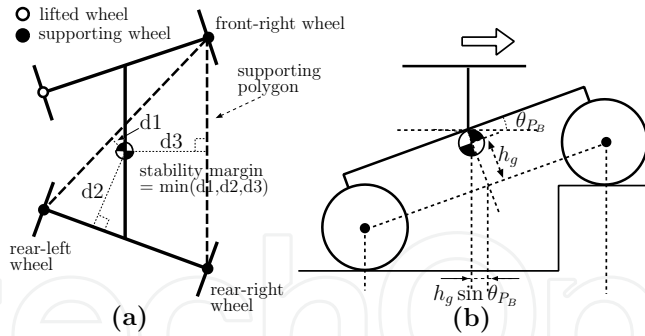


Fig. 13. Stability margin

wheel must be advanced by the minimum distance required for going up the step. Since the lifted wheel can be placed on the step from the state shown in Fig. 14(A-c) by advancing it a distance equal to its radius, θ_A is set at $\tan^{-1}(R'_w / (2A_r))$, where $R'_w = R_w + 0.02[m](\text{margin})$.

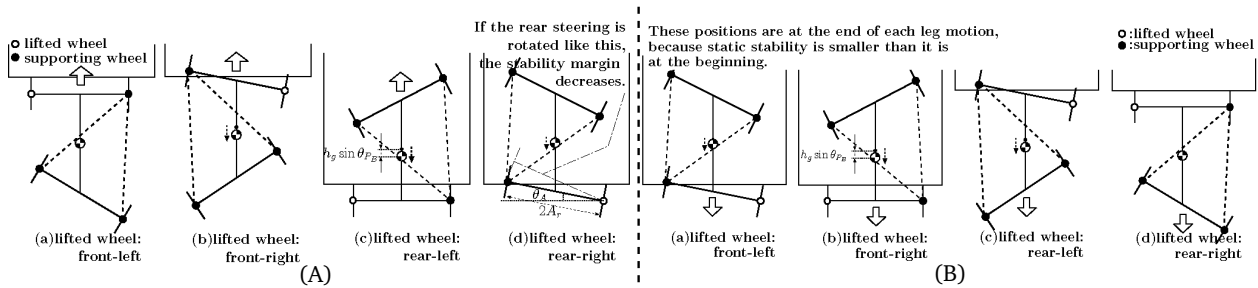


Fig. 14. Four phases during the gait. (A)The step-up gait. (B)The step-down gait.

Since the rear-left wheel is already on the step when lifting the rear-right wheel, the body pitch angle is smaller in (A-d) than in (A-c).

Figure 15 shows the results of numerical calculations of the margin of static stability (the minimum distance between the center of gravity and the supporting polygon) on a 0.15[m] high step. 0.15[m] is the maximum targeted height for the middle size type of RT-Mover.

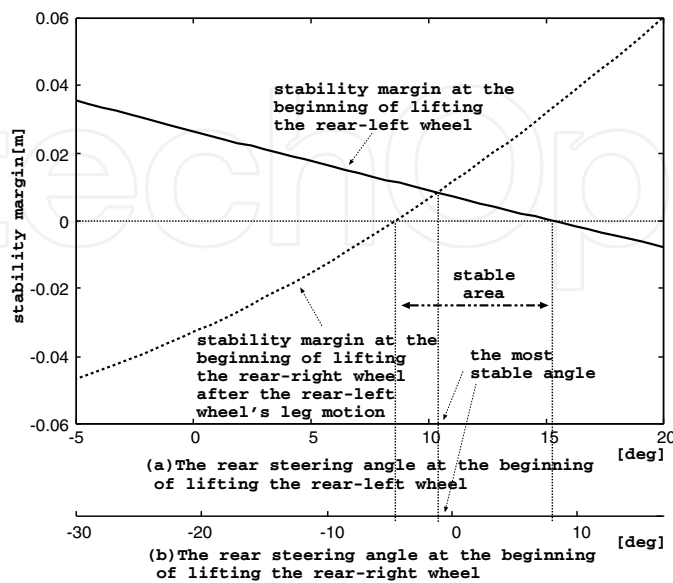


Fig. 15. Static stability data

A positive value of static stability indicates that the robot is stable, and a negative one indicates that it is unstable. Figure 15(a) shows that it is possible to go up a 0.15[m] step while maintaining static stability by setting the rear steering angle to be between 8 and 15.5[deg] when lifting the rear-left leg. The most stable angle is 11[deg], so the yaw angle of the robot becomes 11[deg] in Fig. 9(g).

When descending a step, the four phases in Fig. 14(A) occur in reverse order as shown in Fig. 14(B). The positions shown in Fig. 14(B) are at the end of each leg motion, because static stability is smaller than it is at the beginning. Out of the four phases, only those shown in Fig. 14(B-a) and (B-b) cause static instability due to an inclination of the center of gravity. Because the stability of Fig. 14(B-b) is determined by the condition of Fig. 14(B-a) and Fig. 14(B-a) corresponds to Fig. 14(A-d), Fig. 15(b) can be used for discussing the stability margin for the step-down gait. Figure 15(b) shows that it is possible to go down a 0.15[m] step while maintaining static stability by setting the front steering angle to be between -4.5 and 8[deg] when landing the front-left leg. The most stable angle is -1 [deg].

For the maximum stable angle, the yaw angle of the robot shown in Fig. 10(c) is configured to a value calculated by (A) + (B) + (C). Here, (A) is the maximum stable angle of Fig. 15(b), (B) is the change in front steering angle generated by swinging front-left wheel ($\theta_b - \theta_a$ in Fig. 16), and (C) is the change in the front steering angle generated by the front-left wheel landing (Fig. 16 (c)).

As (A)=-1[deg], (B)=12[deg], and (C)=4[deg] for the robot, the yaw angle of the body is determined to be 15[deg] in Fig. 10(c).

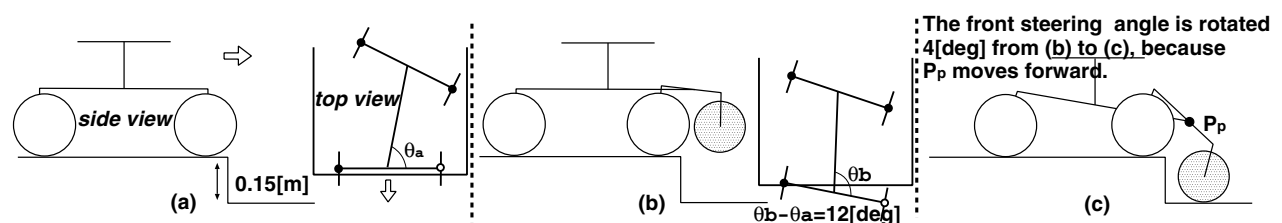


Fig. 16. Change of the front steering angle when moving the front-left wheel forward and lowering it

7. Assessment of ability of locomotion in leg mode

7.1 Step-up gait

The proposed step-up gait was evaluated through a simulation and an experiment. The conditions of the simulation are the following. The upward step height is 0.15[m], the height when lifting a wheel is 0.16[m], the distance that the lifted wheel is moved forward is 0.12[m], the yaw angle of the body relative to the step in Fig. 9(g) is 11[deg], the angular velocity of a roll-adjustment shaft when lifting the wheel is 0.2[rad/s], θ_0 in Fig. 12(c) is 0.2[rad/s], the angular velocity of a roll-adjustment shaft when landing the wheel is 0.1[rad/s], and the forward velocity of the body in wheel mode is 0.1[m/s]. In this chapter, the road shape is assumed to be known in advance. The robot starts 0.2[m] from the step, as shown in Fig. 17. The configured values are given a margin of 0.01[m] when lifting a wheel onto a step of height 0.15[m] and a margin of 0.02[m] when extending the wheel by the wheel radius of 0.1 [m]. The configured value of each process velocity in leg mode is obtained experimentally from a velocity that gives static leg motion. There are plans to address high-speed leg processes for both step-up and step-down gaits in the future.

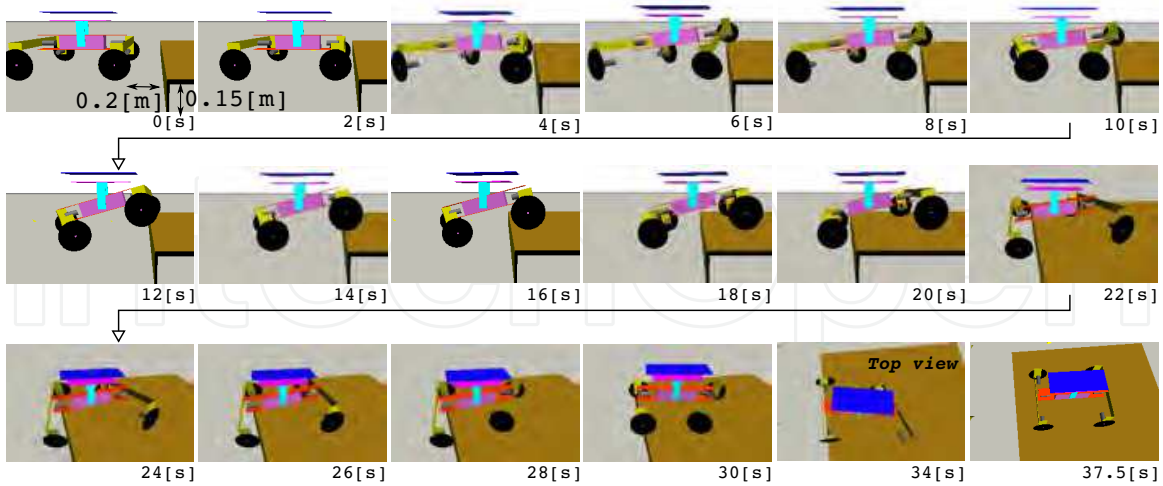


Fig. 17. Snapshots of the step-up gait simulation

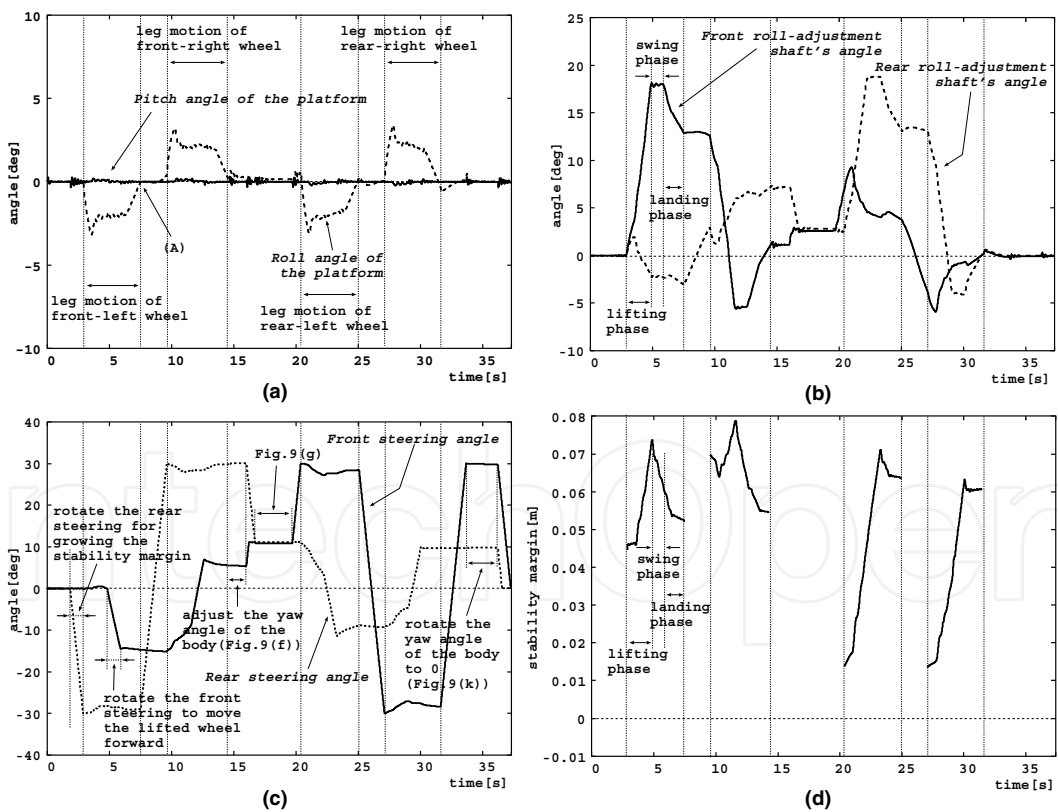


Fig. 18. Simulation data for the step-up gait. (a) Posture angles of the platform. (b) Front and rear roll-adjustment shaft's angles. (c) Front and rear steering angles. (d) Static stability margin during each leg motion.

Figure 18 shows the posture of the platform, the angles of the front and rear roll-adjustment shafts, the front and rear steering angles, and the static stability during each leg motion. Figure 18(a) shows that the pitch posture angle of the platform is almost kept horizontal. The roll angle of the platform is kept horizontal to within $\pm 3[\text{deg}]$. At $2.8 \sim 7.5[\text{s}]$, $9.6 \sim 14.5[\text{s}]$, $20.4 \sim 25.0[\text{s}]$, and $27.1 \sim 31.6[\text{s}]$, the roll angle is larger than at other times because the twisting force around the body, caused by the roll-adjustment shaft that produces the torque for lifting a wheel, disturbs the posture control of the other roll-adjustment shaft. The timings given are those during each leg motion.

Figure 18(b) shows the transition of angles of the front and rear roll-adjustment shafts. From $2.8[\text{s}]$ to $7.5[\text{s}]$, the front-left wheel is lifted. First, the wheel is lifted until the front roll-adjustment shaft is rotated at $18[\text{deg}]$ ($2.8[\text{s}]$ to $4.9[\text{s}]$). From $4.9[\text{s}]$ to $5.9[\text{s}]$, the front steering is rotated until it reaches $-14.5[\text{deg}]$ so that the wheel moves forward $0.12[\text{m}]$ (Fig. 18(c)). Then the wheel moves downward from $5.9[\text{s}]$ to $7.5[\text{s}]$. Since the roll angle of the platform changes from negative to positive at $7.5[\text{s}]$ ((A) in Fig. 18(a)), the landing of the wheel can be detected. The other legs behave similarly.

Figure 18(c) shows the transition of angles of the front and rear steering shafts. From $2.8[\text{s}]$ to $7.5[\text{s}]$, the front wheels are lifted. While the front-left wheel is lifted, the rear steering shaft rotates to its steering limit of $-30[\text{deg}]$ ($1.8[\text{s}]$ to $7.5[\text{s}]$) so that the static stability increases. After lifting the front-left wheel, the wheel is moved forward until the front steering angle becomes $-14.5[\text{deg}]$ ($4.9[\text{s}]$ to $5.9[\text{s}]$). While the front-right wheel is lifted, the rear steering shaft is maintained at the steering limit of $30[\text{deg}]$ ($9.6[\text{s}]$ to $14.5[\text{s}]$) so that the static stability increases. The rear steering shaft is also maintained at $30[\text{deg}]$ ($14.5[\text{s}]$ to $15.9[\text{s}]$) after the front wheels are lifted, thereby adjusting the yaw angle of the body relative to the step to $11[\text{deg}]$ for lifting the rear wheels. Rear wheels are lifted between $20.4[\text{s}]$ and $31.6[\text{s}]$. While the rear-left wheel is lifted, the wheel is moved forward $0.12[\text{m}]$ until the rear steering shaft reaches an angle of $-10.8[\text{deg}]$ ($22.1[\text{s}]$ to $23.1[\text{s}]$). The front steering shaft is rotated to $\pm 30[\text{deg}]$ in order to ensure static stability.

Figure 18(d) shows the data for static stability only during leg motion, because static stability is large enough during wheel mode. The figure shows that the static stability is maintained. When lifting the front-left wheel, the static stability increases, because the center of gravity of the robot moves backward according to the body pitch ($2.8[\text{s}]$ to $4.9[\text{s}]$). In the swing phase of the front-left wheel, static stability decreases, because the position of the front-right wheel with respect to the body changes and the supporting polygon becomes smaller ($4.9[\text{s}]$ to $5.9[\text{s}]$). Finally, in its landing phase, static stability decreases, because the center of gravity of the robot moves forward due to the body pitch ($5.9[\text{s}]$ to $7.5[\text{s}]$).

Figure 19 shows scenes from a step-up gait experiment and the experimental data. The conditions of the experiment are the same as those of the simulation except the D gains for each shaft are set experimentally. The actual robot can also move up onto the $0.15[\text{m}]$ -high step, and the features of the experimental data are almost the same as those of the simulation data. However, it takes about $2.5[\text{s}]$ longer to perform the movement in the experiment than in the simulation. The main reason is that the detection of the landing of each wheel is delayed due to a difference in the posture of the platform between the simulation and the experiment. The inclination of the pitch angle of the platform is larger in the experiment than in the simulation, because of the backlash of the pitch-adjustment shaft and the friction acting on it in the actual robot. Thus, the proposed step-up gait was proved to be effective.

7.2 Step-down gait

The proposed step-down gait was evaluated using a simulation and an experiment. Due to space limitations, only the result of simulation is shown. The conditions of the simulation are the following. The downward step height is 0.15[m], the height when lifting a wheel is 0.02[m], the length the lifted wheel is moved forward is 0.12[m], the yaw angle of the body in Fig. 10(c) is 15[deg], the angular velocity of a roll-adjustment shaft when lifting a wheel is 0.2[rad/s], θ_0 in Fig. 12(c) is 0.2[rad/s], the angular velocity of a roll-adjustment shaft when landing a wheel is 0.1[rad/s], the forward velocity of the body in wheel mode is 0.1[m/s], and the road shape is known in advance. The robot starts at a position 0.2[m] from the step, as shown in Fig. 20. The configured value allows a margin of 0.02[m] in the height by which to lift the wheel and in the length by which to swing the lifted wheel forward. The configured value of each process velocity in leg mode is obtained experimentally from a velocity that gives static leg motion.

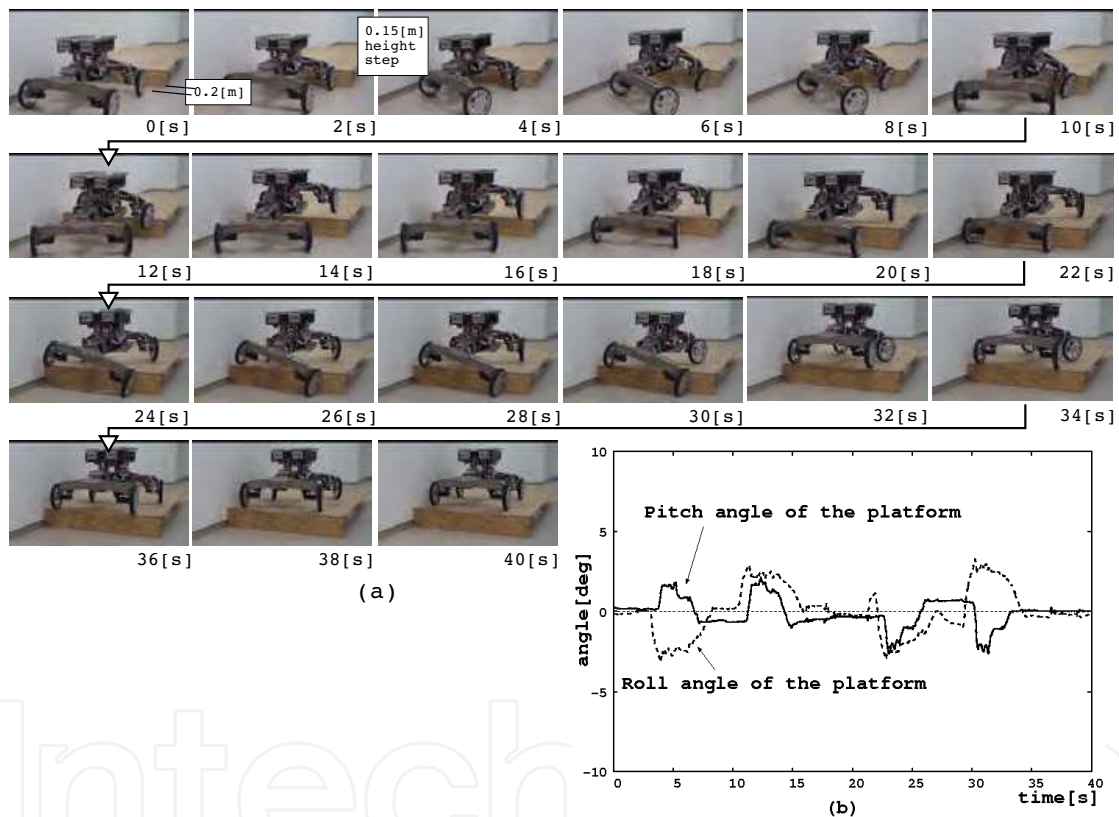


Fig. 19. Experimental data for the step-up gait. (a) Experimental scenes. (b) Posture angles of the platform.

Figure 20 shows snapshots of the step-down gait simulation. It can be seen that the step-down gait presented in Fig. 10 is performed stably.

8. A personal mobility vehicle, RT-mover P-type

RT-Mover P-type (Fig. 21) that is one of RT-Mover series is introduced. This robot can carry a person even if on the targetted rough terrain. The specifications of it are listed in Table 5. When rotating the roll-adjustment axis through 30[deg] such that the wheel on one side is in contact with the ground, the other wheel attached to a 0.65[m] steering arm can rise

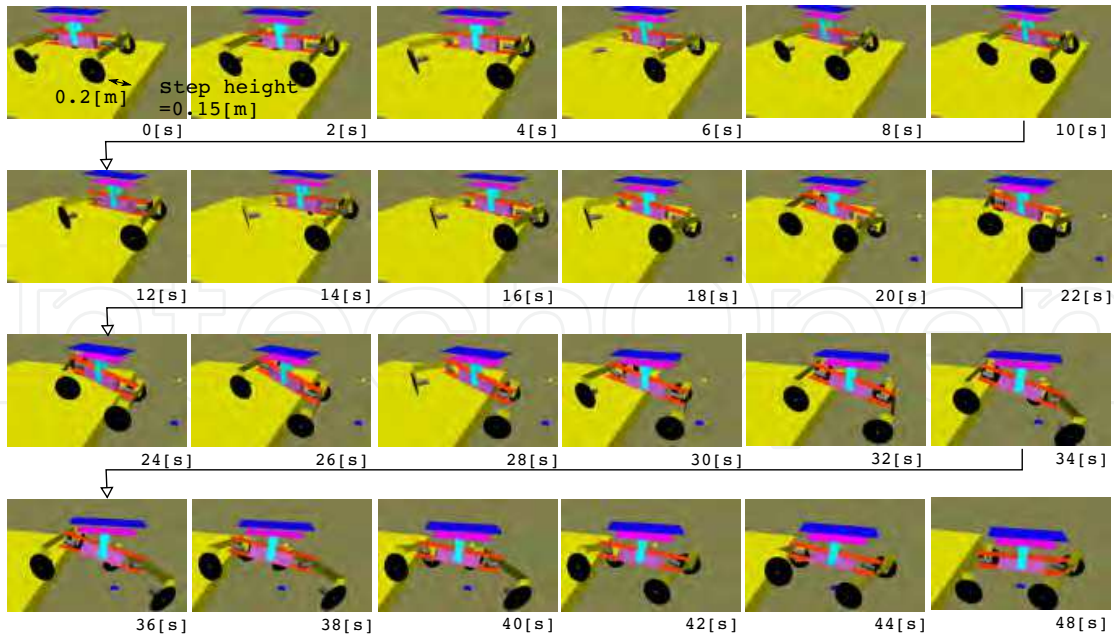


Fig. 20. Snapshots of the step-down gait simulation

0.325[m]. Therefore, the movement range is sufficient for the targeted terrain. Likewise, moving 0.325[m] in the front and rear directions is possible by moving the steering from 0[deg] to 30[deg], and holes of 0.325[m] can be crossed. With regards to locomotion on a slope, back-and-forth movement and traversal of a slope of up to 30[deg] is possible.

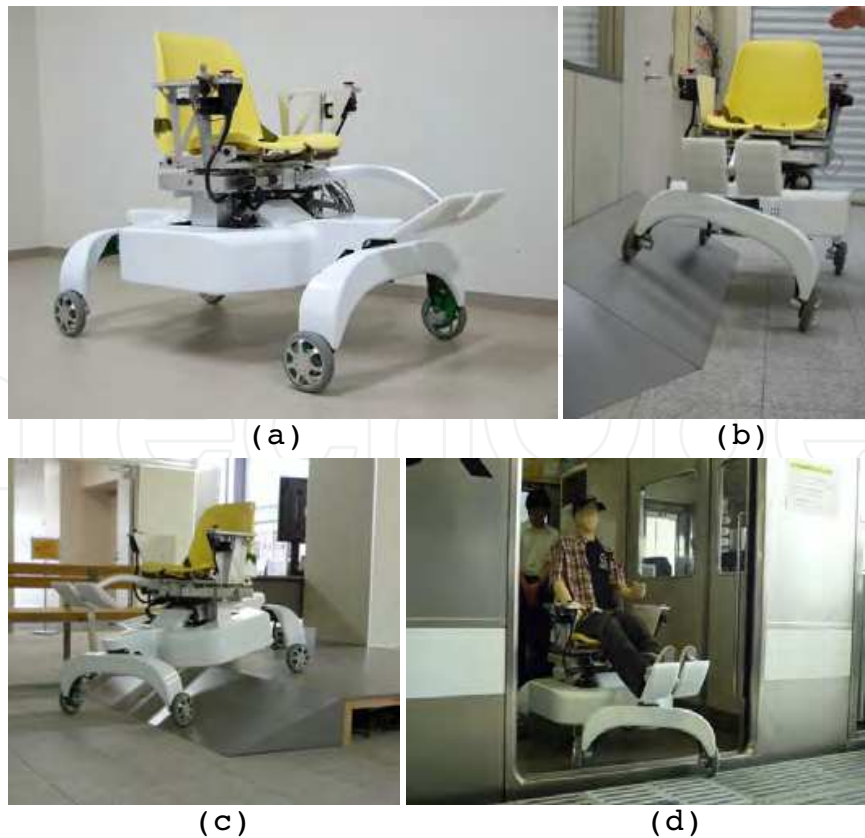


Fig. 21. (a)RT-Mover P-type. (b)On a bank. (c)On a slope. (d)Getting off a train.

Dimensions	Length 1.15[m](excluding footrest); Width 0.70[m] (Tread 0.60[m]); Height to seat 0.58[m]; Height to bottom 0.17[m]
Wheel	Radius:0.15[m]; Width:0.03[m]
Weight	80[kg] (including batteries at 20[kg])
Motor	maxon brushless motor 100[W] × 9
Gear ratio	100 (each wheel, front and rear steering); 820 (pitch-adjustment shaft); 2400 (roll-adjustment shaft)
Sensor	Encoder (each motor); Current sensor (each motor); Posture angle sensor (roll and pitch of platform)
Angle limit	± 30 [deg] (steering, roll-adjustment shaft, and pitch-adjustment shaft)
Max speed	4.5[km/s]
Power supply	48[V] lead accumulator

Table 5. Main specifications of P-type

In fact, additional motors are attached to the robot, for example, for adjusting footrest mechanism. Those are, however, not essential functions for moving on rough terrain, so they are not discussed here.

9. Assessment of ability of locomotion of P-type

Evaluations were performed through experiments taking a step-up gait and a step-down gait as examples. The above-mentioned methodology is also used for these gaits. At the current stage, road shapes are known in advance.

Fig.22 shows data of the step-up walking experiment over a 0.15[m]-high step. The robot can get over a 0.15[m] step with a person riding on it while maintaining the horizontal position of its platform within ± 5 [deg]. The main conditions are the followings. The angular velocity of a roll-adjustment shaft when lifting and landing the wheel are 0.2[rad/s] and 0.1[rad/s]

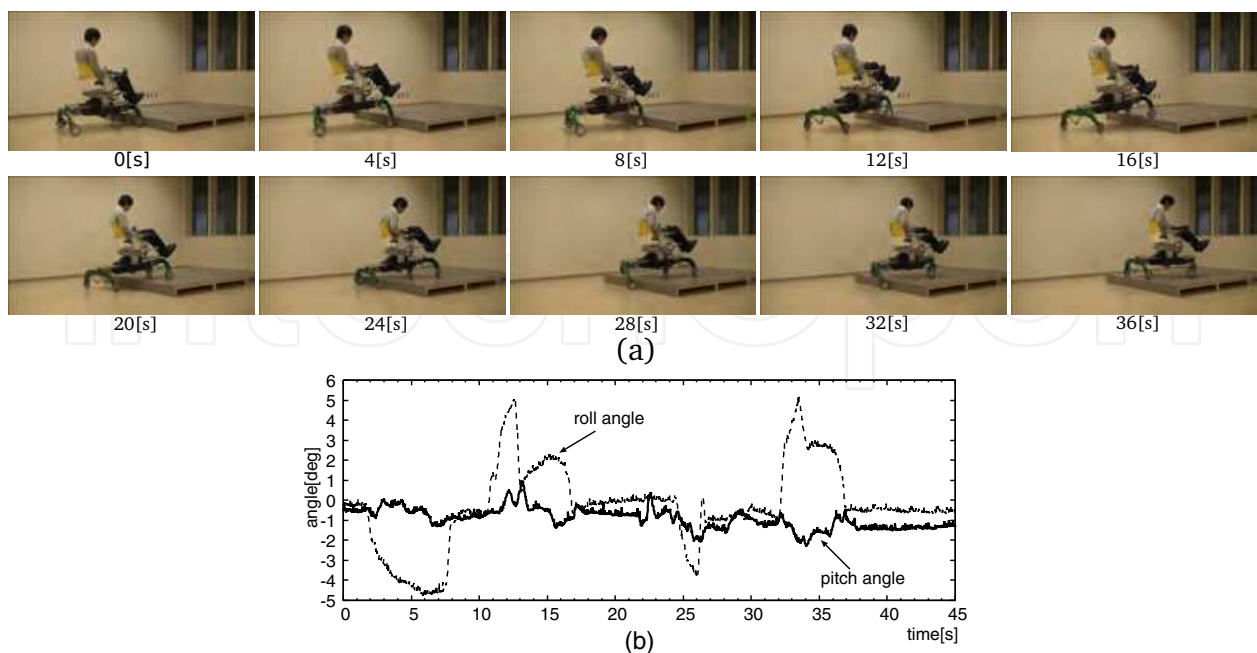


Fig. 22. Experimental result of the step-up gait. (a)Snapshots. (b)Posture angles of the platform.

respectively, that of a steering shaft to put forward the lifted leg is $0.2[\text{rad/s}]$, and the forward velocity of the body in wheel mode is $0.12[\text{m/s}]$. The configured value of each process velocity in leg mode is obtained experimentally from a velocity that gives static leg motion. There are plans to address high-speed leg processes in near future.

Fig.23 shows data of the step-down walking experiment down a $0.15[\text{m}]$ -high step. The main conditions are basically the same as the step-up gait experiment. The robot can decline a $0.15[\text{m}]$ step with a person riding on it while maintaining the horizontal position of its platform within $\pm 4.5[\text{deg}]$.

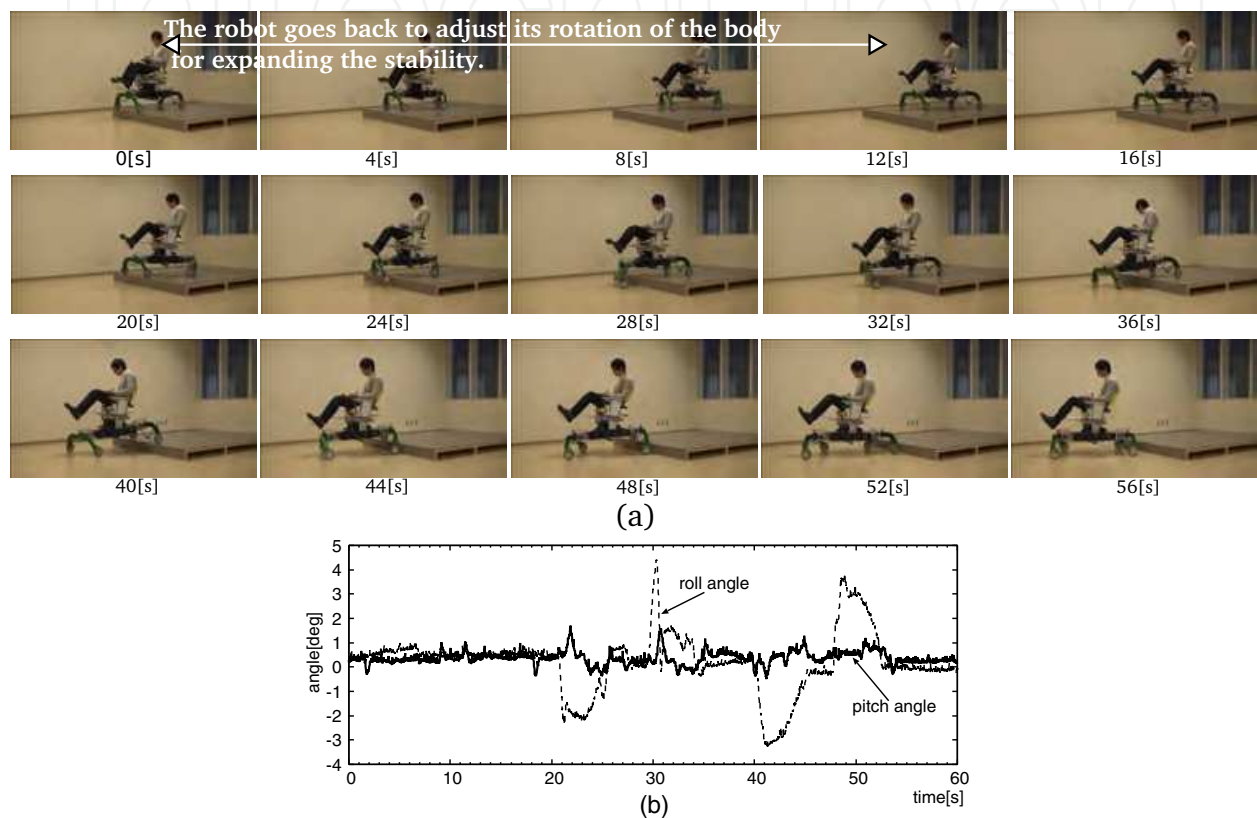


Fig. 23. Experimental result of the step-down gait. (a)Snapshots. (b)Posture angles of the platform.

10. Conclusions

We have developed some mobile platforms with leg-wheel mechanism for practical use, including a real size personal mobility vehicle (Fig. 24(a)). They are RT-Movers that have both of a wheel mode and a leg mode in a simple mechanism. They have four drivable wheels and two leg-like axles. The wheels are mounted on one side of the leg-like axles at the front and rear of the body. The mechanism is realized with few drive shafts to achieve the minimum necessary leg functions, taking a four-wheel model as the base.

The mechanical design concept was discussed and strategies for moving on rough terrain were proposed. The kinematics, stability, and control method of RT-Mover were also described in detail. Some typical cases of wheel mode and leg mode locomotion were selected, and the robot's ability of locomotion on rough terrain was assessed through simulations and

experiments. In every case, the robot was able to move while maintaining the horizontal position of its platform.

We are undertaking joint research with a railway company to develop a personal mobility robot for outdoor use, including on rough terrain. Good coordination between the personal mobility robot and the railway system may also lead to a new type of transportation system (see Fig. 24(b)).

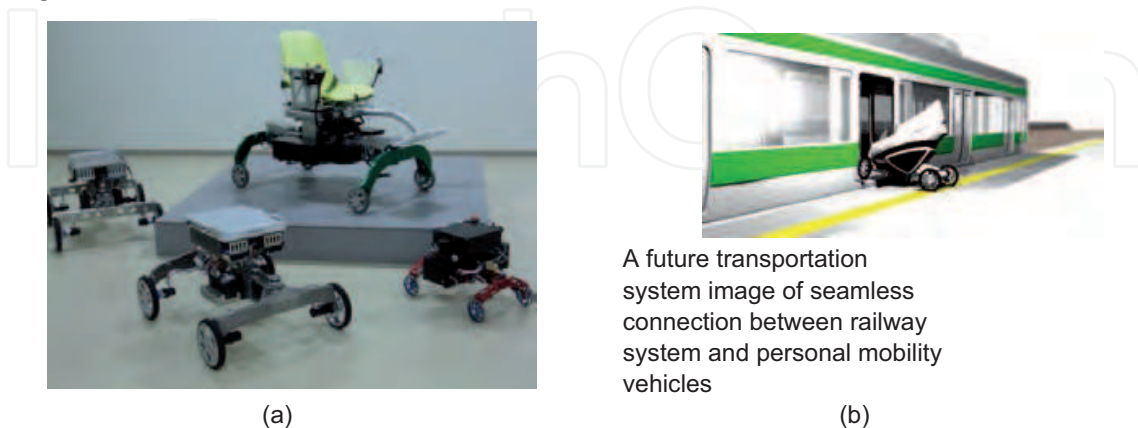


Fig. 24. Snapshots. (a) RT-Mover series. (b) A future transportation system image.

Since this research has just started, there is much work that should be done in the future, for example: 1. allowing for the perception of rough terrain rather than moving over obstacles whose position is known in advance; 2. adapting control methods for moving on different types of rough terrain; 3. dynamic control on rough terrain for high-speed locomotion.

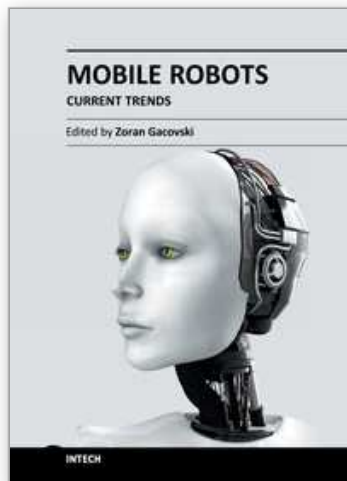
11. References

- Bares J. and Wettergreen D., (1997). Lessons from the development and deployment of Dante II, *Proceedings of the 1997 Field and Service Robotics Conference*, pp.72-79.
- Daltorio K. A., et al., (2009). Mini-Whegs Climbs Steep Surfaces Using Insect-inspired Attachment Mechanisms, *The International Journal of Robotics Research*, 28(2): 285-302.
- Delcomyn F. and Nelson M. E., (2000). Architectures for a biomimetic hexapod robot, *Robotics and Autonomous Systems*, 30: 5-15.
- Endo G. and Hirose S., (2000). Study on roller-walker (multi-mode steering control and self-contained locomotion), *Journal of Robotics and Mechatronics*, 12(5): 559-566.
- Grand C., et al., (2004). Stability and Traction Optimization of a Reconfigurable Wheel-Legged Robot, *The International Journal of Robotics Research*, 23(10-11): 1041-1058.
- Halme A., et al., (2003). WorkPartner: Interactive Human-Like Service Robot for Outdoor Applications, *The International Journal of Robotics Research*, 22(7-8): 627-640.
- Hirose S., et al., (1985). The Gait Control System of the Quadruped Walking Vehicle, *Journal of the Robotics Society of Japan*, 3(4): 304-323.
- Kimura H., et al., (2007). Adaptive Dynamic Walking of a Quadruped Robot on Natural Ground Based on Biological Concepts, *The International Journal of Robotics Research*, 26(5): 475-490.
- Kubota T., et al., (2003). Small, light-weight rover "Micro5" for lunar exploration, *Acta Astronautica*, 52: 447-453.
- Lacagnina M., et al., (2003). Kinematics, dynamics and control of a hybrid robot Wheeleg, *Robotics and Autonomous Systems*, 45: 161-180.

- Lauria M., et al., (1998). Design and control of an innovative micro-rover, *Proceedings of the Fifth ESA Workshop on Advanced Space Technologies for Robotics and Automation*, The Netherlands, 1998.
- Morales R., et al., (2006). Kinematic Model of a New Staircase Climbing Wheelchair and its Experimental Validation, *The International Journal of Robotics Research*, 25(9): 825-841.
- Nakajima S., (2011). RT-Mover: a rough terrain mobile robot with a simple leg-wheel hybrid mechanism, *The International Journal of Robotics Research*, doi:10.1177/0278364911405697 .
- Nakajima S., (2011). Development of a Personal Mobility Robot for Rough Terrain, *Proceedings of the 14th CLAWAR*, accepted.
- Nakajima S. and Nakano E., (2008a). Adaptive Gait for Large Rough Terrain of a Leg-wheel Robot (First Report: Gait Strategy), *Journal of Robotics and Mechatronics*, 20(5): 801-805.
- Nakajima S. and Nakano E., (2008b). Adaptive Gait for Large Rough Terrain of a Leg-wheel Robot (Second Report: Step-Up Gait), *Journal of Robotics and Mechatronics*, 20(6): 913-920.
- Nakajima S. and Nakano E., (2009a). Adaptive Gait for Large Rough Terrain of a Leg-wheel Robot (Third Report: Step-Down Gait), *Journal of Robotics and Mechatronics*, 21(1): 12-19.
- Nakajima S. and Nakano E., (2009b). Adaptive Gait for Large Rough Terrain of a Leg-wheel Robot (Fourth Report: Step-Over Gait), *Journal of Robotics and Mechatronics*, 21(2): 285-292.
- Nakajima S. and Nakano E., (2009c). Adaptive Gait for Large Rough Terrain of a Leg-wheel Robot (Fifth Report: Integrated Gait), *Journal of Robotics and Mechatronics*, 21(3): 419-426.
- Quaglia G., et al., (2010). The Epi.q-1 Hybrid Mobile Robot, *The International Journal of Robotics Research*, 29(1): 81-91.
- Quinn R. D., et al., (2003). Parallel Complementary Strategies for Implementing Biological Principles into Mobile Robots, *The International Journal of Robotics Research*, 22(3): 169-186.
- Sato M., et al., (2007). An Environmental Adaptive Control System of a Wheel Type Mobile Robot for the Rough Terrain Movement, *Proceedings of the 2007 IEEE/RSJ International Conference on Intelligent Robots and Systems*, pp.3962-3967.
- Siegwart R., et al., (2002). Innovative design for wheeled locomotion in rough terrain, *Robotics and Autonomous Systems*, 40: 151-162.
- Six K. and Kecskem'ethy A., (1999). Steering properties of a combined wheeled and legged striding excavator, *Proceedings of the 10th World Congress on the Theory of Machines and Mechanisms*, pp.135-140.
- Smith J. A., et al., (2006). PAW: a Hybrid Wheeled-Leg Robot, *Proceedings of the 2006 IEEE International Conference on Robotics and Automation*, pp.4043-4048.
- Song S. M. and Waldron K. J., (1989). *Machines That Walk: The Adaptive Suspension Vehicle*, MIT Press.
- Thuerer T., et al., (2006). CRAB-Exploration rover with advanced obstacle negotiation capabilities, *Proceedings of the 9th ESA Workshop on Advanced Space Technologies for Robotics and Automation*, pp.1-8.
- Volpe R., et al., (1997). Rocky 7: A next generation Mars rover prototype, *Journal of Advanced Robotics*, 11(4): 341-358.

- Winnendael M. V., et al., (1999). Nanokhod micro-rover heading towards Mars, *Proceedings of the Fifth International Symposium on Artificial Intelligence, Robotics and Automation in Space*, pp.69-76.
- Yoneda K., (2007). Light Weight Quadruped with Nine Actuators, *Journal of Robotics and Mechatronics*, 19(2): 160-165.
- Yoneda K., et al., (2009). High-grip Stair Climber with Powder-filled Belts, *The International Journal of Robotics Research*, 28(1): 81-89.
- Yuan J. and Hirose S., (2004). Research on Leg-wheel Hybrid Stair Climbing Robot, Zero Carrier, *Proceedings of the 2004 IEEE International Conference on Robotics and Biomimetics*, pp.1-6.

IntechOpen



Mobile Robots - Current Trends

Edited by Dr. Zoran Gacovski

ISBN 978-953-307-716-1

Hard cover, 402 pages

Publisher InTech

Published online 26, October, 2011

Published in print edition October, 2011

This book consists of 18 chapters divided in four sections: Robots for Educational Purposes, Health-Care and Medical Robots, Hardware - State of the Art, and Localization and Navigation. In the first section, there are four chapters covering autonomous mobile robot Emmy III, KCLBOT - mobile nonholonomic robot, and general overview of educational mobile robots. In the second section, the following themes are covered: walking support robots, control system for wheelchairs, leg-wheel mechanism as a mobile platform, micro mobile robot for abdominal use, and the influence of the robot size in the psychological treatment. In the third section, there are chapters about I2C bus system, vertical displacement service robots, quadruped robots - kinematics and dynamics model and Epi.q (hybrid) robots. Finally, in the last section, the following topics are covered: skid-steered vehicles, robotic exploration (new place recognition), omnidirectional mobile robots, ball-wheel mobile robots, and planetary wheeled mobile robots.

How to reference

In order to correctly reference this scholarly work, feel free to copy and paste the following:

Shuro Nakajima (2011). Mobile Platform with Leg-Wheel Mechanism for Practical Use, Mobile Robots - Current Trends, Dr. Zoran Gacovski (Ed.), ISBN: 978-953-307-716-1, InTech, Available from: <http://www.intechopen.com/books/mobile-robots-current-trends/mobile-platform-with-leg-wheel-mechanism-for-practical-use>

INTECH
open science | open minds

InTech Europe

University Campus STeP Ri
Slavka Krautzeka 83/A
51000 Rijeka, Croatia
Phone: +385 (51) 770 447
Fax: +385 (51) 686 166
www.intechopen.com

InTech China

Unit 405, Office Block, Hotel Equatorial Shanghai
No.65, Yan An Road (West), Shanghai, 200040, China
中国上海市延安西路65号上海国际贵都大饭店办公楼405单元
Phone: +86-21-62489820
Fax: +86-21-62489821

© 2011 The Author(s). Licensee IntechOpen. This is an open access article distributed under the terms of the [Creative Commons Attribution 3.0 License](#), which permits unrestricted use, distribution, and reproduction in any medium, provided the original work is properly cited.

IntechOpen

IntechOpen